# Density and Surface Texture Measurements of 3D Printed Sand to Improve Modeling

Samuel R. Morris
Department of Mechanical Engineering, University of Maine, Orono, Maine, USA

Philip F. King, Ph.D.
Department of Mechanical Engineering, University of Maine, Orono, Maine, USA
Advanced Structures and Composites Center, University of Maine, Orono, Maine, USA



## ABSTRACT

Within the field of 3D sand printing, there is a growing need to understand the anisotropic behavior of sand in the build envelope of 3D sand printers. For metalcasting, this understanding will improve mold accuracy and design. This work provides methodologies to characterize printed sand's density and surface texture as related to orientation within a printer build envelope, two properties that directly impact liquid metal flow and solidification. Density of printed sand samples was found to vary based on the travel direction of the printer recoater. Surface roughness was found to be influenced by multiple factors, each changing the surface roughness by up to 13%. These findings highlight the importance of considering anisotropy in the design of 3D printed sand molds. The methodologies developed in this study provide a foundation for future research aimed at improving the modeling of complex 3D printed sand molds.

**Keywords**: additive manufacturing, 3D sand printing, 3DSP, material properties, process modeling, mold design

## INTRODUCTION

3D Sand printing (3DSP) has revolutionized the sand-casting industry. In addition to the design freedom it enables, it has also enabled casting to be economical for small job and batch production runs.[1-7] Another transformational technology that has been deployed in sand casting in the last 30 years has been numerical modeling of filling and solidification.[8–11] Modeling has transformed the mold design process by providing designers and engineers with a tool to predict potential defects prior to investing in tooling.[12] As the complexity of cores and molds has risen, it is increasingly necessary to better characterize and describe the printers that produce them, up to and including the variations in printed parts' physical properties throughout the build volume of the printer.

The 3DSP process is inherently different from traditional mold-making techniques even when the same materials are used (same sand and binder), and computational modeling must take this into account. Traditional mold making uses sand that is mixed with the binder and activator and then packed around the pattern, either by hand or with a press. 3DSP, on the other hand, is a binder jet process that uses a roller to pack each layer, and then applies the binder to the select locations that will comprise the mold.[13,14] Even though the materials used in the two processes are the same, these differences in the mold making process have the potential to impact how the sand is packed, which in turn can change the bulk properties of the mold. Consequently, to have accurate modeling, the material properties of 3D printed sand molds must be fully understood.

The 3DSP process is known to be anisotropic, with properties varying along the x, y, and z directions of the printed parts. Prior research has investigated how part orientation in the printer impacts the mechanical properties (flexural strength) and permeability,[12] while other research has studied the effect of part orientation on surface roughness.[15]

Previous work in this field has noted the general anisotropy of 3D printed materials.[16,17] Other work has provided dilatometry results for phenol resin-bonded printed samples,[18] demonstrating the changes in the thermal properties of sand molds with a change in manufacturing process. Recent work by Bedel et al.[15] established a relation between surface texture and orientation within a printer's build volume, plotting roughness against horizontal angle and developing a corresponding transfer function for arithmetic average roughness (Ra), as well as determining a predictive function for the final cast surface roughness.

This paper aims to further study the anisotropy of 3D printed molds with a focus on improving modeling by increasing the understanding of the roughness and density

of printed sand molds. In addition to expanding the literature on the effect of part orientation on bulk properties, this work also examines how the properties vary within a single specimen based on that specimen's orientation. The work presented in this paper provides methods to characterize sand printers and improve sand casting process modeling.

## METHODS

### SAMPLE PREPARATION

Samples were printed with Covia Incast 80 foundry sand[19] using a commercial binder jet printer with a 0.016 inch (400 micron) layer height and 6.6% average binder content. The binder used was a proprietary organic binder. Three sample geometries were used: a rectangular prism measuring 1.18 x 1.18 x 1.97 inches (3 x 3 x 5 centimeters), a rectangular prism measuring 1.18 x 1.18 x 3.94 in. (3 x 3 x 10 cm.), and a right triangular prism measuring 1.18 x 1.18 x 1.97 in. (3 x 3 x 5 cm.) as in Figure 1. The particle size distribution for the foundry sand is in Table 1.

***Table 1. Printed Sand Particle Size Distribution***

| Mesh Size | | Mean % Retained |
|---|---|---|
| ASTM | Microns | |
| 50 | 300 | 2.2 |
| 70 | 212 | 14.7 |
| 100 | 150 | 47.5 |
| 140 | 106 | 28.8 |
| 200 | 75 | 6.4 |
| 270 | 53 | 0.4 |

Samples were arranged in the print volume such that each geometry had a group of samples with their short axis aligned with the print envelope's x-axis and another group with their short axis aligned with the y-axis. The printer's recoater travels along the x-axis. The short rectangular prism samples also had a group of samples located at a higher z-height in the print volume. The number of samples in each sample group are relayed in Table 2.

Sample groups were given alphanumeric reference codes, which are used in the following figures. The first character indicates short axis alignment; "A" for alignment with the x-axis, "B" for the y-axis. The second character indicates either sample shape or z-height; "0" for triangular prism samples, "1" for low z-height, "2" for high z-height. A third character indicates relative size; "S" for short, "L" for long.

Thus, a high z-height short rectangular prism sample with its short axis aligned with the x-axis would be in group code A2S. Group codes are in parentheses in Table 2 entries.

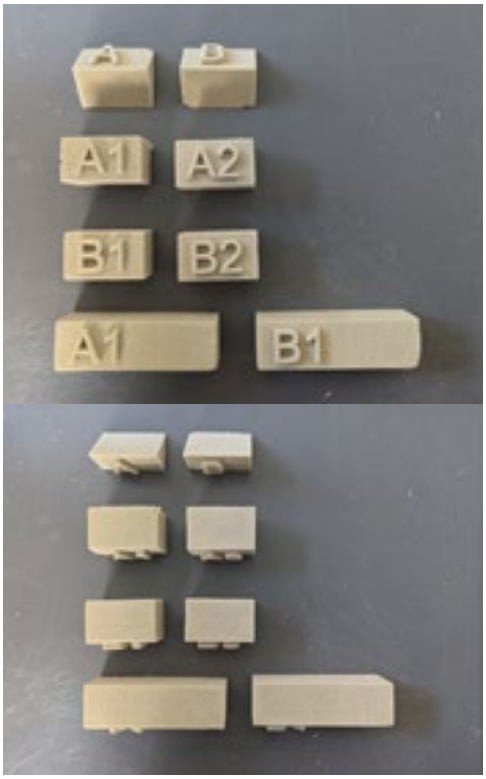


***Figure 1. Two views of representative samples.***

### DENSITY MEASUREMENTS

Short rectangular prism samples were x-rayed with a Quintek Measurement Systems QDP-01X 40 keV vertical density profilometer, at a resolution of 0.002 inches (50.8 microns) per step. Samples were scanned in a direction perpendicular to their long axis (Figure 2).

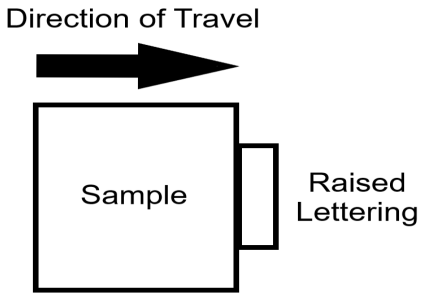


***Figure 2. Direction of X-ray scanner travel.***

***Table 2. Sample Group Populations and Naming Scheme***

| Type | Right Triangular | Long Rectangular | Short Rectangular (Low z-height) | Short Rectangular (High z-height) |
|---|---|---|---|---|
| Total | 12 | 11 | 12 | 18 |
| Aligned with x-axis | 6 (A0S) | 6 (A1L) | 7 (A1S) | 5 (A2S) |
| Aligned with y-axis | 6 (B0S) | 5 (B1L) | 8 (B1S) | 10 (B2S) |

## ROUGHNESS MEASUREMENTS

Samples were imaged by a Keyence VHX-7000 digital microscope with an E20 lens at 20x magnification. Surface texture measurements were performed using the microscope's onboard software, applying wavelength limits for the Gaussian filtering function according to ASME B46.1.[20] For area profiles, the short wavelength limit was 50 microns, with a long wavelength limit of 8 mm; for linear profiles, the short wavelength limit was 25 microns, with a long wavelength limit of 8 mm.

Profiles were measured at five separate locations each on two faces of the short and long rectangular prism samples (faces were orthogonal to Face 1 and coplanar with Face 2 the z-axis of the print volume), and three separate locations on a single face of the right triangular prism samples (face was angled at 45° relative to horizontal), Figure 3. Area profiles were measured over an approximately 0.264 inches square (170 mm square) area. Linear profiles were measured across the measured area's horizontal and vertical centerlines over a 0.315 inch (8 mm) distance.

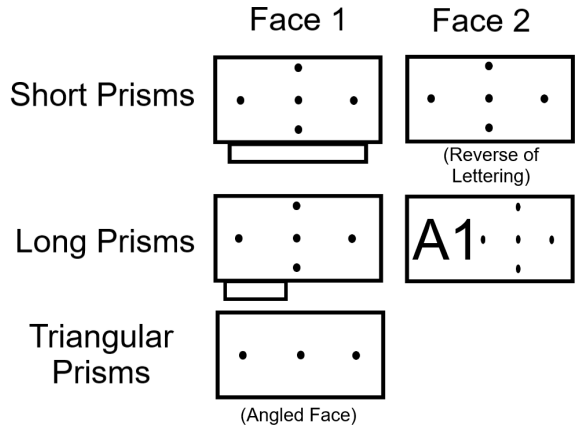


***Figure 3. Roughness sampling areas sorted by sample type and selected face.***

## STATISTICAL ANALYSIS

### Density Measurements

Samples were compared as two groups based on their long axis orientation. The area of analysis was trimmed to produce correlation residuals of 0.5 lb/ft3 or 0.5% in the group mean density distributions, minimizing edge effects. Significantly lower density at the edges of measured regions was observed in all samples. Trimmed groups were compared with a two-tailed paired student T-test with $\alpha = 0.05$ and a null hypothesis of equal means.

### Roughness Measurements

Within the three main sample populations, comparisons were made between groups based on long axis orientation, z-height for the short samples, and selected face for the long and short samples. Between the populations, comparisons were made between applicable internal groups for the effect of sample length and face orientation on surface texture. Arithmetic mean roughness (Sa and Ra) was the parameter of interest. Comparisons of mean Sa/Ra were made using a two-sample, two-tailed student t-test with $\alpha = 0.05$, with the variance being compared with a two-sample, one tail f-test with $\alpha = 0.05$. The null hypothesis for the t-tests was zero difference between means; null hypothesis for the f-tests was equal variances.

Additionally, an Analysis of Variance (ANOVA) with $\alpha = 0.05$ was performed to test if the Sa along the length of the samples varied. The samples oriented along the x-axis were tested separately from the samples oriented along the y-axis to determine if sample orientation played a role in the potential variance of roughness.

# RESULTS AND DISCUSSION

## DENSITY MEASUREMENTS

Mean densities of the two groups of short rectangular prism samples are shown in Figure 4. A difference in the density of samples along the x- and y-axes was indicated in the comparisons of the longitudinal density distributions and the mean group densities. The rate of change of density along the length of samples, however, was found to be similar.

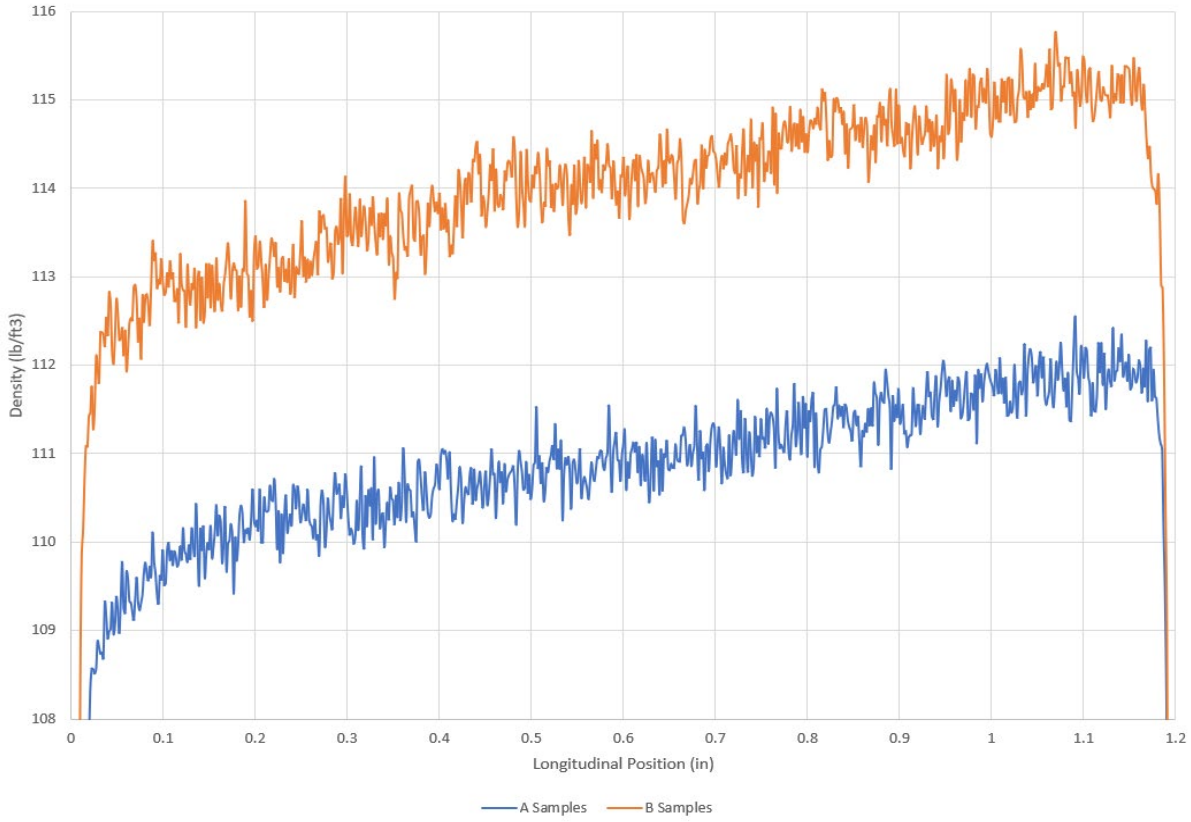


***Figure 4. Mean density distributions for short rectangular prism samples with their short axes aligned with the x-axis (A samples) and with the y-axis (B samples)***

Samples' densities tended to rise on average 2 lb/ft$^3$ per inch (13 kg/m$^3$ per cm) of print length in the direction of scanning, approximately 102% of initial density. It should be noted again that the printer's recoater travels along the x-axis; the scan direction when aligned with the x-axis was opposite the print direction. The difference in density between print and y-axis directions was approximately 2.5% on average, with the y-axis tending to have a higher mean density.

These findings have several implications. First, they further confirm the anisotropy of 3DSP, and the binder jet additive manufacturing process, in general. However, these findings also suggest that the printhead control strategy impacts the characteristics of the printed molds and cores. For the densities measured along the y-axis of the samples, an initial conjecture after observing an increase in density across the samples is that either the build plate or recoater is not level, leading to a difference in compaction along the y-axis. This cannot be the case, however, because the samples were distributed across the build volume of the printer, but all showed a similar relative change in density. If the change in density was caused by the build plate or recoater not being level, a linear change in density that continues across the entire y-axis of the printer (i.e., samples printed at $y = 0$ have low density, samples printed at $y = \infty$ have high density, or vice versa) might be expected instead. Similarly, the density difference measured along the print direction of the samples cannot be explained by build plate or recoater leveling because they too showed similar relative changes in densities.

What might explain the increase in density along both the x- and y-axes of the samples is the printhead control strategy. Whenever the printhead of a printer switches on to deposit binder there is a delayed pressure increase within the printhead followed by a large initial release of binder and then a slow ramp-down of binder flow. In the print direction, this ramp-down could lead to more binder being initially deposited, raising the density at the samples' leading edge. In the y-direction if the signal being applied to the printheads activates them in a certain direction, there could be a delay in activation, leading to a variation in density along the samples' y-axis.

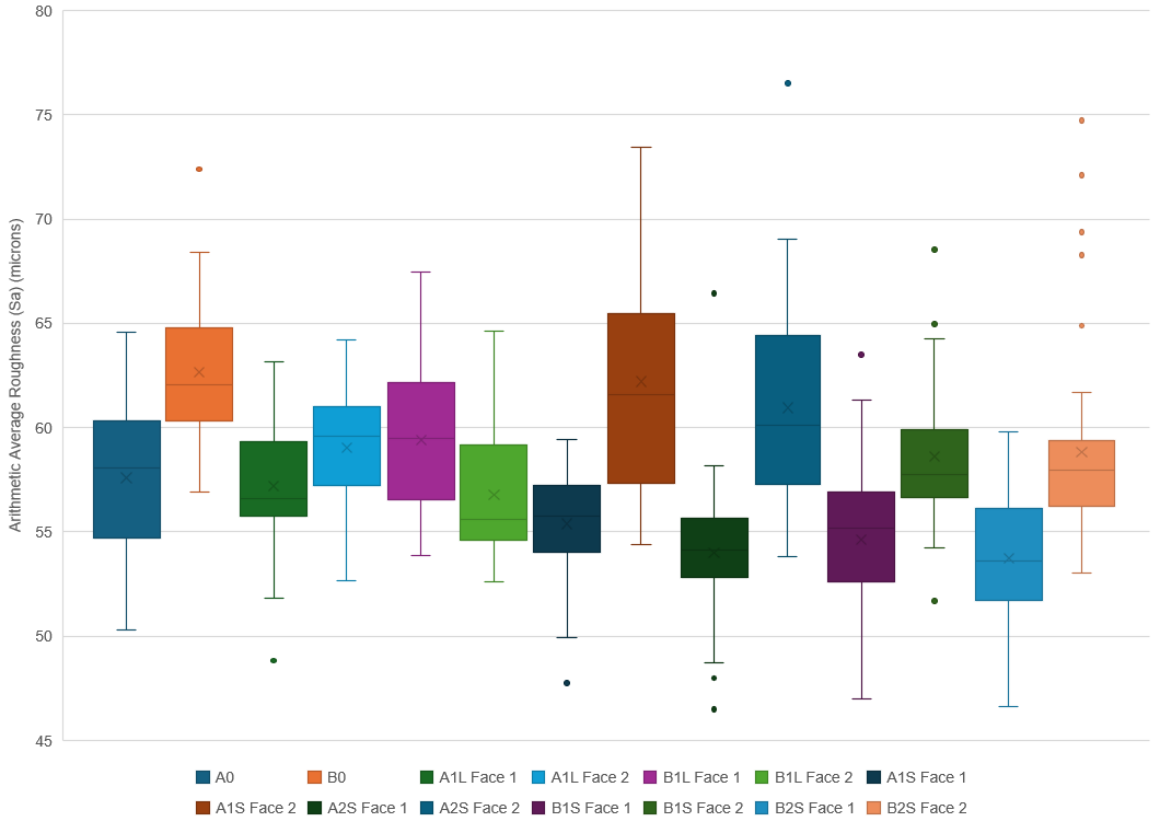


***Figure 5. Arithmetic Average Roughness (Sa) distributions for all sample groups.***

These hypotheses suggest that the source of decreased density in the print direction and increased density in the y-direction is a decrease in binder deposition along the x-axes and an increase in binder deposition along the y-axes of the samples. If so, gas evolution from the binder will vary in different sections of the molds depending on their orientation within the build volume, potentially affecting final casting properties. As a result, users of printed molds should consider how they orient and position their prints within the build volume to ensure they do not inadvertently increase gas defects in critical sections of castings.

## ROUGHNESS MEASUREMENTS

The results of linear profile measurements are not considered in the following discussion because of their high variance with measurement location due to the directional nature of the measurement method. A more accurate representation of the surface morphology is achieved with the area profile measurements because of the high resolution of the digital microscope's area profile which does not rely on an average set of linear profiles, as opposed to other measurement methods.

The area roughness (Sa) distributions of the groups of samples as they were compared with each other is in Figure 5.

The influence of long axis orientation on roughness was demonstrated for all sample groups except for Face 1 of the short rectangular prism samples printed higher in the build volume with their short axes oriented along the x-axis as compared to short rectangular prism samples with their short axes oriented along the y-axis ($p = 0.93$). Samples with short axes oriented along the x-axis tended to have higher roughness. The influence of z-height was only demonstrated for Face 1 of short rectangular prism samples ($p = 0.049$). The influence of face orientation, specifically between 0° and 90° relative to horizontal in long and short rectangular prism samples, was demonstrated. Face 2 tended to have higher roughness. The influence of face orientation between all three sample groups was demonstrated except for the long rectangular prism and right triangular prism samples with their short axes oriented along the x-axis ($p = 0.70$ for Face 1 of the long rectangular prism samples, $p = 0.16$ for Face 2). The angled face of the right triangular prism samples tended to be rougher. The influence of sample length was demonstrated between long and short rectangular prism samples. Long samples tended to have higher roughness on Face 1, while shorter samples tended to have higher roughness on Face 2. Finally, for all the samples, Sa did not vary along their lengths, whether with respect to the x- or y-axes.

These findings offer several insights into the anisotropic nature of 3DSP. As has been reported previously,[15] side surfaces, angled surfaces, and top surfaces each have different roughness, with the angled surfaces having overall greater roughness due to the stair-stepping effect.

Other findings showed that the orientation of the samples (along x- and y-axes) had an impact on the surface roughness even when the measured faces were coplanar, and that the long samples had different roughness than the short samples. On their own, these results do not reveal much, but when examined with the results of the density measurements in mind they lead to the following hypotheses.

The difference in roughness due to orientation could result from the ramp of the printheads. Due to size limitations of the vertical density profilometer, only the short samples' densities could be measured. As was stated previously, the densities decreased along the print direction and increased along the y-axes of the samples. However, it is expected that the density will not continue to trend linearly but will level off once the printhead finishes ramping. For the samples oriented with their short axis parallel to the y-axis of the printer, the binder deposition may have inconsistently reached full binder saturation, while the samples oriented with their short axis parallel to the x-axis of the printer may have reached full binder saturation.

The influence of sample length for the top sides of the samples can also be explained by this same phenomenon. The longer samples have more of their volume at full binder saturation which could lead to different surface morphologies. The difference in the side surface roughness is most likely due to the way the measurements were taken. The short samples were measured on the back side (side recoater last encounters) and the long samples were measured on the front side (side recoater first encounters). While this invalidates results pertaining to the influence of sample length on side surface roughness, it does suggest that back surfaces will have different roughness than front surfaces. This is hypothesized to be a result of the front surface experiencing sand moving toward it due to the action of the recoater while the back surface experiences sand being pulled away from it.

## CONCLUSION

Anisotropy in additive manufacturing is universal. For high-monetary-investment printers, such as 3DSP printers, it becomes increasingly important to characterize the effects of orientation and location within that specific printer's build volume to more effectively model and slice increasingly complex and precise geometries. The methodologies discussed in this work enable a user to characterize the density variations within the print volume, which directly affects the thermal properties of the sand-binder mixture, as well as the surface roughness of various part orientations, which affects both the flow properties and the final surface finish of a casting. With knowledge of both properties' variations, a user may position their core or mold for both optimum density and surface finish, subject to the normal solidification concerns of any casting.

Future work will focus on the production of larger samples, to confirm the density increase seen in this work, and on correlating density and surface roughness with exact location within a printer's build volume. Characterization of thermal properties, modeling optimization, and casting trials will also be performed in later works.

## REFERENCES

1. Martinez, D. et al., "Effect of freezing range on reducing casting defects through 3D sand-printed mold designs," *The International Journal of Advanced Manufacturing Technology* (2023). doi:10.1007/s00170-023-11112-x
2. Sama, S.R., Badamo, T., Lynch, P. & Manogharan, G., "Novel sprue designs in metal casting via 3D sand-printing," *Additive Manufacturing* **25**, 563–578 (2019).
3. Sama, S.R., Wang, J. & Manogharan, G., "Non-conventional mold design for metal casting using 3D sand-printing," *Journal of Manufacturing Processes* **34**, 765–775 (2018).
4. Shangguan, H. et al., "3D-printed shell-truss sand mold for aluminum castings," *Journal of Materials Processing Technology* (2017). doi:10.1016/j.jmatprotec.2017.05.010
5. Walker, J.M. et al., "Real-time process monitoring of core shifts during metal casting with wireless sensing and 3D sand printing," *Additive Manufacturing* **27**, 54–60 (2019).
6. Walker, J. et al., "3D Printed Smart Molds for Sand Casting," *International Journal of Metalcasting* **12**, 785–796 (2018).
7. Upadhyay, M., Sivarupan, T. & El Mansori, M., "3D printing for rapid sand casting—A review," *Journal of Manufacturing Processes* **29**, 211–220 (2017).
8. Sulaiman, S. & Hamouda, A.M.S., "Modelling and experimental investigation of solidification process in sand casting," *Journal of Materials Processing Technology* **155–156**, 1723–1726 (2004).
9. Desai, P., Berry, J. & Kim, C., "Computer simulation of forced and natural convection during filling of a casting," *AFS Transactions* **92**, 519 (1984).

10. Cross, M. & Campbell, J., "Modeling of casting, welding and advanced solidification processes" VII. (1995).
11. Lin, H.-J. & Hwang, W.-S., "Combined fluid flow and heat transfer analysis for the filling of casting," *Modeling and Control of Casting and Welding Processes, IV* 487–511 (1988).
12. Coniglio, N., Sivarupan, T. & El Mansori, M., "Investigation of process parameter effect on anisotropic properties of 3D printed sand molds," *Int J Adv Manuf Technol* **94**, 2175–2185 (2018).
13. Sachs, E., Cima, M., Williams, P., Brancazio, D. & Cornie, J., "Three Dimensional Printing: Rapid Tooling and Prototypes Directly from a CAD Model," *Journal of Engineering for Industry* **114**, 481–488 (1992).
14. Ziaee, M. & Crane, N.B., "Binder jetting: A review of process, materials, and methods," *Additive Manufacturing* **28**, 781–801 (2019).
15. Bedel, M., Fabre, A. & Coniglio, N., "Defining the printing direction impact of additively manufactured sand molds on casting roughness," *Journal of Manufacturing Processes* **116**, 329–340 (2024).
16. Ahn, S., Montero, M., Odell, D., Roundy, S. & Wright, P.K., "Anisotropic material properties of fused deposition modeling ABS," *Rapid Prototyping Journal* **8**, 248–257 (2002).
17. Zou, R. et al., "Isotropic and anisotropic elasticity and yielding of 3D printed material," *Composites Part B: Engineering* **99**, 506–513 (2016).
18. Saeidpour, M., Svenningsson, R., Gotthardsson, U. & Farre, S., "Thermal Properties of 3D-Printed Sand Molds," *Inter Metalcast* **16**, 252–258 (2022).
19. Covia Corp., "Incast Foundry Sand Technical Data Sheet."
20. American Society of Mechanical Engineers, "B46.1-2019: Surface Texture (Surface Roughness, Waviness, and Lay)" (2020).